Reentrant localization and mobility edges in a spinful Aubry-André-Harper model with a non-Abelian potential

Enguo Guan,[1,2] Gang Wang,[3] Xi-Wen Guan,[1,4,5] and Xiaoming Cai[1,*]

[1]*Innovation Academy for Precision Measurement Science and Technology, Chinese Academy of Sciences, Wuhan 430071, China*
[2]*University of Chinese Academy of Sciences, Beijing 100049, China*
[3]*School of Physical Science and Technology, Soochow University, Suzhou 215006, China*
[4]*NSFC-SPTP Peng Huanwu Center for Fundamental Theory, Xi'an 710127, China*
[5]*Department of Fundamental and Theoretical Physics, Research School of Physics and Engineering, Australian National University, Canberra ACT 0200, Australia*

(Received 28 May 2023; accepted 16 August 2023; published 6 September 2023)

We study localization properties and mobility edges of a generalized spinful Aubry-André-Harper (AAH) model, which is the dimensional reduction of the two-dimensional Hofstadter model with a non-Abelian SU(2) gauge potential. Depending on whether the quasiperiod is comparable with the lattice size, the model has different localization properties. In the noncomparable case, the generalized AAH model still retains duality properties. Tuning the non-Abelian gauge can make the system undergo an unconventional reentrant localization phase transition as the strength of quasiperiodic potential increases. Furthermore, mobility edges exist in the mixed phase where the localized states sit at the center of spectra. Nevertheless, the non-Abelian gauge potential results in more mobility edges than that the Abelian gauge potential does, when the model is in the semiclassical limit where the quasiperiod is comparable with the lattice size. Moreover, exact expressions of the mobility edges and localization phase diagrams are analytically obtained by a semiclassical method.

DOI: 10.1103/PhysRevA.108.033305

I. INTRODUCTION

The Aubry-André-Harper (AAH) model [1,2] has become a workhorse for studying quantum localization and topological insulators in one dimension (1D). It originates from the dimensional reduction of the two-dimensional (2D) Hofstadter model [3], describing electrons in the 2D square lattice subjecting to an Abelian gauge potential, which is usually generated by a uniform magnetic field. Inheriting the topological nature of the Chern insulator, it supports the Thouless pumping [4–6]. When the strength of magnetic field is a finite irrational number, the reduced AAH model is quasiperiodic and supports a localization phase transition. It undergoes a transition from a completely extended phase to a completely localized phase at a finite strength of quasiperiodic potential, ensured by a self-duality [1,3,7]. However, in the infinitesimal case, a slowly varying quasiperiodic potential gives rise to exact mobility edges, which can be obtained by an analytical semiclassical calculation [8]. The mobility edge, which acts as a characteristic of energy, separates the localized and extended eigenstates in the whole spectra [9,10]. It is crucial in understanding various fundamental phenomena, such as the metal-insulator transition and controlled transport [11], heat engine [12], energy current rectification [13–15], superradiant instability [16], and even the many-body localization [17]. Such a system with the mobility edge displays a strong thermoelectric response which can be used in thermoelectric devices [11,12,18].

By introducing short- [19] or long-range hopping terms [20], spin-orbit coupling [21,22], or the modified quasiperiodic potentials breaking the self-duality of the classic AAH model [23–25], one can obtain mobility edges in generalized AAH models. However, very few of them support exact expressions of mobility edges [26–30]. Besides mobility edges, it was reported recently that, in the 1D dimerized lattice with a staggered quasiperiodic potential, some of the localized single-particle states become extended for an intermediate potential strength [19]. This system undergoes an unconventional reentrant localization, i.e., the extended-mixed-localized-mixed-localized phase transition. In parallel, some generalized AAH models with slowly varying potentials have been extensively studied [31–34] on the localization and mobility edges. The AAH model and some of its extensions have been experimentally realized in a variety of systems, such as ultracold atoms [17,35–40] and photonic crystals [4,41].

The concept of gauge potential is at the heart of modern high-energy physics and has become a fuel for research. Quantum simulations of gauge potentials have been pursued for decades and have resulted in new developments of lattice gauge theories [42–47]. In this paper, we study localization properties and mobility edges of a generalized spinful AAH model, which is a dimensional reduction of the 2D Hofstadter model subjected to a non-Abelian SU(2) gauge potential. Although the Abelian gauges have been well studied and simulated, the non-Abelian ones like the SU(2) gauge are

*cxmpx@wipm.ac.cn

still an on-going topic, the underlying study of which was mainly restricted to numerical simulations [48]. Here, we focus on the AAH model with a non-Abelian gauge potential and study effects of the non-Abelian SU(2) gauge potential on localization. These were rarely discussed in literature [21,22,49]. Given the criticality of the comparability between the quasiperiod and the lattice size, we consider both noncomparable and comparable cases. In the noncomparable case with a finite irrational number, by tuning the non-Abelian gauge, the system produces the reentrant localization transition and the mixed phase where the mobility edge can exist. Besides, the generalized spinful AAH model still has duality. We give the localization phase diagrams, which are decided by the duality. On the other hand, we analytically study the localization properties and mobility edges of the model in the semiclassical limit where the quasiperiodic potential is slowly varying (the comparable case with an infinitesimal irrational number). The non-Abelian gauge induces more mobility edges than the Abelian one. Exact expressions of the mobility edges and the localization phase transition points are obtained, which crucially depend on strengths of the non-Abelian gauge potential.

The rest of paper is organized as follows. In Sec. II, we introduce the generalized AAH model, from the dimensional reduction of the 2D Hofstadter model subjected to non-Abelian SU(2) gauge potentials. Section III is devoted to the study of duality, (reentrant) localization, and mobility edges for the AAH model with a noncomparable quasiperiodicity. Derivation of the exact expressions of mobility edges and corresponding numerical verifications for the model with slowly varying potentials are presented in Sec. IV. Finally, we conclude our main results and present a short discussion on experimental realizations in Sec. V.

II. MODEL AND HAMILTONIAN

It is well known that the classic AAH model is the dimensional reduction of the 2D Hofstadter model, describing electrons hopping in the square lattice threaded by a homogeneous magnetic field corresponding to Abelian U(1) gauge potentials. Here we consider two-component particles in the square lattice subjected to a synthetic gauge potential

$$\boldsymbol{A} = (\alpha\sigma_y, 2\pi\Omega m\sigma_0 + \beta\sigma_x). \tag{1}$$

$\sigma_{0,x,y}$ are Pauli operators in the two-component pseudospin subspace. Ω is the strength of the Abelian U(1) gauge potential. α and β represent strengths of non-Abelian SU(2) gauge fluxes along the x and y directions, respectively. Such a gauge potential may be realized by laser-assisted spin-dependent hopping [42,50,51]. The Hamiltonian of the generalized Hofstadter model is

$$\begin{aligned} H_{\mathrm{Hof}} = & -\sum_{m,n} \Psi^{\dagger}_{m+1,n} J_x e^{i\alpha\sigma_y} \Psi_{m,n} \\ & -\Psi^{\dagger}_{m,n+1} J_y e^{i\beta\sigma_x + i2\pi\Omega m} \Psi_{m,n} + \mathrm{H.c.} \end{aligned} \tag{2}$$

$\Psi^{\dagger}_{m,n} = (\psi^{\dagger}_{m,n,\uparrow}, \psi^{\dagger}_{m,n,\downarrow})$ is the creation operator at lattice site (m, n). m and n are indexes of sites along the x and y directions respectively. $J_{x(y)}$ are hopping amplitudes along the two directions. Because of the presence of translational symmetry in the y direction where a periodic boundary condition is employed, one can introduce a partial Fourier transformation and obtain the dimensional reduction of the generalized Hofstadter model, i.e.,

$$\begin{aligned} H(\alpha, \beta) = & -J_x \sum_m \left[\Psi^{\dagger}_m \begin{pmatrix} \cos\alpha & -\sin\alpha \\ \sin\alpha & \cos\alpha \end{pmatrix} \Psi_{m+1} + \mathrm{H.c.} \right] \\ & -2J_y \sum_m \Psi^{\dagger}_m \begin{bmatrix} \cos\beta\cos(2\pi\Omega m + k_y) & -\sin\beta\sin(2\pi\Omega m + k_y) \\ -\sin\beta\sin(2\pi\Omega m + k_y) & \cos\beta\cos(2\pi\Omega m + k_y) \end{bmatrix} \Psi_m, \end{aligned} \tag{3}$$

which is a generalized spinful AAH model. After performing the partial Fourier transformation, J_x is the hopping amplitude for the generalized AAH model, and we will set it as the unit of energy ($J_x = 1$). J_y, corresponding to the hopping amplitude in y direction, becomes the strength of the quasiperiodic potential and the momentum k_y turns into a global phase, which is trivial on localization. Thus we will set $k_y = 0$ without loss of generality. Here we set $\Psi^{\dagger}_m = (\psi^{\dagger}_{m\uparrow}, \psi^{\dagger}_{m\downarrow})$, which is the creation operator at site m. $\uparrow$ and $\downarrow$ denote two pseudospins (hyperfine levels) or legs in a ladder. Ω is an irrational number, characterizing the quasiperiodicity of potential. Due to the periodicity of trigonometric functions, we can restrict $\Omega \in (0, 1)$. The model has parity-time symmetry but not parity and time-reversal symmetries themselves when $k_y = 0$, and eigenstates are doubly degenerate.

The localization of the AAH model is crucially dependent on the comparability between the quasiperiod $1/\Omega$ and the lattice size L, which are two characteristic lengths of the model besides the underlying lattice constant. For a finite Ω, we usually have $1/\Omega \ll L$, i.e., the quasiperiod is noncomparable with the lattice size. In the noncomparable case, the quasiperiodic potential is incommensurate to the underlying lattice, and the whole lattice contains many quasiperiods. Then, the quasiperiodic potential acts as a pseudodisorder and induces localization. On the other hand, in the semiclassical limit with an infinitesimal Ω, we have $1/\Omega \simeq L$, i.e., the quasiperiod is comparable with the lattice size. The quasiperiodic potential loses its incommensurability to the underlying lattice and is slowly varying spatially. But the potential still can induce localization which can be analytically studied by a semiclassical method. In the thermodynamic limit, one needs to choose $L \to \infty$ and also $\Omega \to 0$ in the comparable case, while only $L \to \infty$ in the noncomparable case. For completeness, there is another trivial case with $1/\Omega \gg L$,

where the quasiperiodic potential can be treated as a constant potential.

The model has localization symmetries regarding both α and β. First, $H(\alpha, \beta)$ and $H(\alpha, \beta + \pi)$ only differ by a phase shift $k_y \to k_y + \pi$, and they share the same localization behavior regardless of k_y. Otherwise, $H(\alpha + \pi, \beta)$ is mapped to $H(\alpha, \beta)$, by sending Ψ_m to $(-1)^m \Psi_m$. On the other hand, $H(-\alpha, \beta)$ and $H(\alpha, \beta)$ are related by the parity symmetry which sends Ψ_m to Ψ_{-m}, and $H(\alpha, -\beta)$ is mapped to $H(\alpha, \beta)$ by sending Ψ_m to $\sigma_z \Psi_{-m}$. Because of these symmetries, we restrict both α and β to the interval $[0, \pi/2]$.

When $\alpha\beta = 0$, the model reduces to two decoupled copies of the classic AAH model, whose localization properties essentially depend on the irrational number Ω. When Ω is finite, the system undergoes a metal-insulator phase transition at a finite strength of the quasiperiodic potential, which is guaranteed by a self-duality. The system is in the extended phase where all single-particle states are extended when $J_y < 1$, whereas it is in the localized phase with all localized states when $J_y > 1$. When $\Omega \ll 1$, semiclassical analyses showed that the model supports exact mobility edges $|E| = |1 - J_y|$ when $J_y < 1$. States with energies E lying between these two mobility edges are extended; otherwise, they are localized. That $\alpha\beta \neq 0$ is the focus of our study. In the next section, duality and localization of the model with finite Ω will be discussed. Semiclassical analyses on localization and exact mobility edges are presented in Sec. IV.

III. DUALITY AND REENTRANT LOCALIZATION FOR FINITE Ω

In this section, we focus on localization properties of the model with finite Ω, whose quasiperiod is noncomparable with the lattice size ($1/\Omega \ll L$). To initiate our analyses, we perform a Fourier transformation of Eq. (3) with $k_y = 0$, which allows us to express the Hamiltonian in the dual space in terms of the creation operator $\Psi^\dagger_{k_x} = (\psi^\dagger_{k_x\uparrow}, \psi^\dagger_{k_x\downarrow})$. The equation is

$$H^* = -J_y \sum_{k_x} \left[\Psi^\dagger_{k_x} \begin{pmatrix} \cos\beta & -\sin\beta \\ \sin\beta & \cos\beta \end{pmatrix} \Psi_{k_x+1} + \text{H.c.} \right] - 2J_x \sum_{k_x} \Psi^\dagger_{k_x} \begin{bmatrix} \cos\alpha\cos(2\pi\Omega k_x) & -\sin\alpha\sin(2\pi\Omega k_x) \\ -\sin\alpha\sin(2\pi\Omega k_x) & \cos\alpha\cos(2\pi\Omega k_x) \end{bmatrix} \Psi_{k_x}. \tag{4}$$

We note that H and H^* share the same mathematical structure, except that the coefficients are interchanged. So the generalized AAH model still has duality. In other words, a localized (extended) state with energy E for the system with $(J_x, J_y, \alpha, \beta)$ corresponds to an extended (localized) state with the same energy E for the system with $(J_y, J_x, \beta, \alpha)$. The model is self-dual when $J_x = J_y$ and $\alpha = \beta$. Otherwise, the self-dual point does not exist.

Next, we use numerical methods to analyze the localization properties. Here, Ω is taken as the golden ratio $(\sqrt{5} - 1)/2$. In practice, it is approximated by rational numbers $\Omega = F_{n-1}/F_n$ with F_n the nth Fibonacci number, and the number of lattice sites $L = F_n$. To characterize localization of a state, one usually uses two well-known quantities, i.e., the inverse of the participation ratio (IPR) and fractal dimension (FD). For a normalized single-particle state, the IPR is defined by $P = \sum_{m\sigma} |\phi_{m\sigma}|^4$ [19,21,52], with $\phi_{m\sigma}$ the single-particle wave function. In general, the IPR $P \propto L^{-\zeta}$, where ζ is the FD. For an extended state, $P \propto 1/L$ with $\zeta = 1$, whereas the IPR approaches 1 and $\zeta = 0$ for a localized state. In the middle, a state with $0 < \zeta < 1$ is critical and has a self-similarity. In Fig. 1(a), we present typical FDs in the (J_y, E) plane, whose values are indicated by colors. FDs of states are extracted numerically by the box-counting method [53]. Furthermore, we present corresponding distributions of IPRs in Fig. 1(b). When the strength J_y of the quasiperiodic potential is small the system is in the extended phase where all $P \propto 1/L, \zeta \simeq 1$, and states are extended, whereas it is in the localized phase for a large enough J_y where all $\zeta \simeq 0$, IPRs are finite, and states are localized. In the intermediate region, it is in the mixed phase, consisting of a finite portion of extended and localized states. Moreover, in the mixed phase, the system

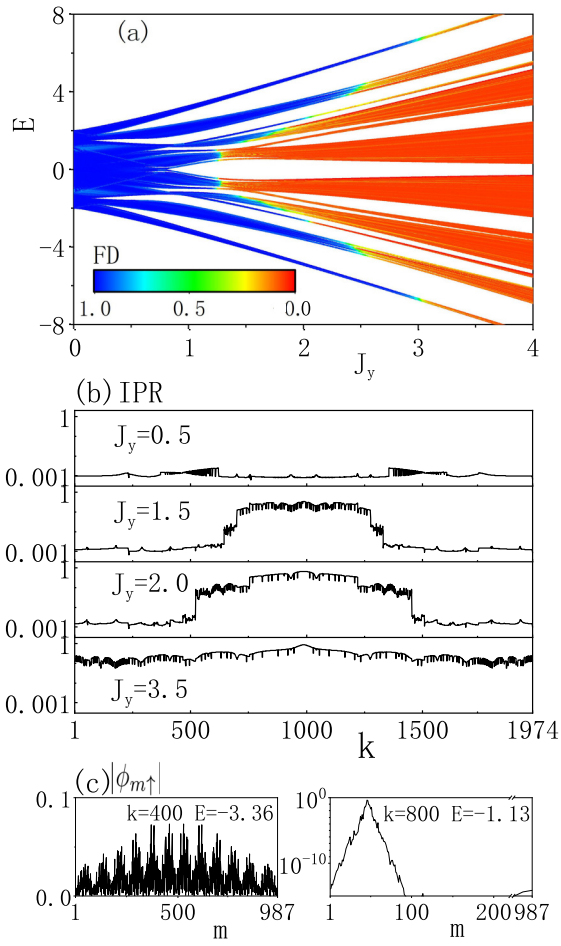

FIG. 1. (a) FDs of single-particle states, as functions of the corresponding energies E and quasiperiodic potential strength J_y, for systems with $\alpha = 1$ and $\beta = \pi/2$. (b) Semilogarithmic plots of the distributions of IPRs for systems with the same $\alpha = 1$ and $\beta = \pi/2$ but different strengths of quasiperiodic potential. k is the index of states, which are arranged in the ascending order of energies. (c) Typical spatial distributions of states, for the system with $J_y = 2$. The irrational number $\Omega = (\sqrt{5} - 1)/2 \simeq 610/987$, and the total number of lattice sites $L = 987$.

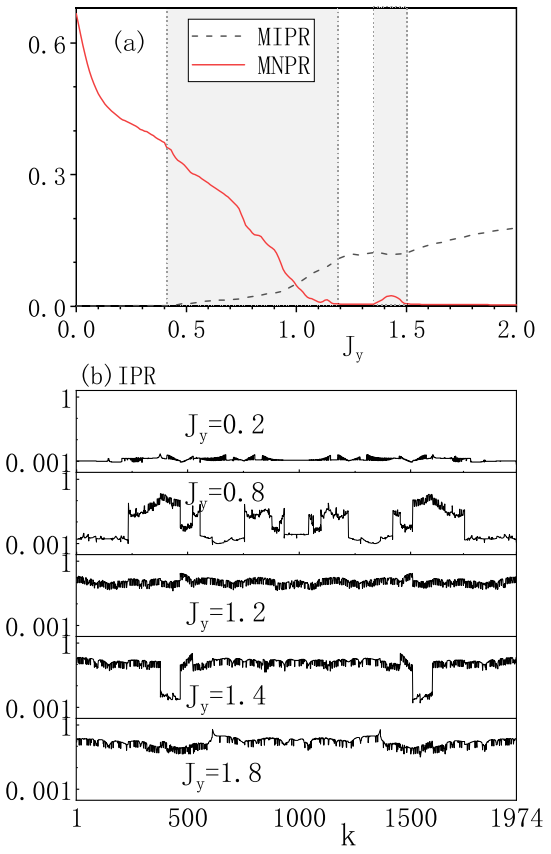

FIG. 2. (a) MIPR and MNPR vs J_y for the system with $\alpha = 0.4\pi$ and $\beta = 0.34\pi$. (b) Semilogarithmic plots of the distributions of IPRs for the same system but with different strengths of quasiperiodic potential. $\Omega \simeq 610/987$ and $L = 987$.

hosts mobility edges, critical energies separating extended and localized states in the spectrum. In distributions of IPRs (FDs) where states are arranged in the ascending order of energies, sudden jumps of them are characteristic features of the presence of mobility edges. There are two mobility edges, and in between them states are exponentially localized, while outside states are extended [see Fig. 1(c) for typical spatial distributions of states]. Two mobility edges, which form at the center of spectrum, move towards the edges of spectrum when the strength J_y increases, and the system thus turns into the localized phase if J_y is large enough.

Besides the normal extended-mixed-localized phase transition, the model also supports the unconventional reentrant localization transition, i.e., the extended-mixed-localized-mixed-localized phase transition, when J_y increases. Besides the IPR, we also use the normalized participation ratio (NPR), which is defined by the "inverse" of IPR for a single-particle state [NPR $= (\text{IPR} \times L)^{-1}$]. Thus, opposite to IPR, NPR $\propto 1/L$ for a localized state, whereas it approaches 1 for an extended state. To further characterize the localization of the whole system, we define the mean inverse of the participation ratio (MIPR) MIPR $= \sum_k \text{IPR}_k/2L$ and the mean normalized participation ratio (MNPR) MNPR $= \sum_k \text{NPR}_k/2L$, averaging over all single-particle states with k the index. For a finite value, MIPR (MNPR) highlights the presence of localized

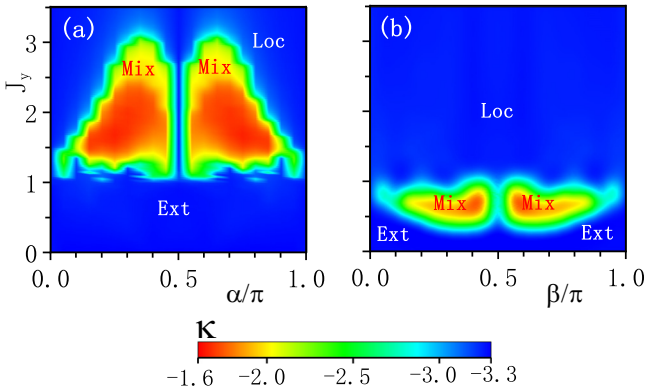

FIG. 3. Contour plot of the quantity κ in Eq. (5), which represents localization phase diagram, for the system with $\beta = 0.5\pi$ (a) or $\alpha = 0.5\pi$ (b). $\Omega \approx 610/987$ and $L = 987$.

(extended) states. Both of them are finite when the system is in the mixed phase, whereas only one of them is finite when the system is in the extended or localized phase. In Fig. 2(a) we present the MIPR and MNPR for the system hosting reentrant localization transition. Correspondingly, we show distributions of IPRs at different J_y in Fig. 2(b). Two gray regions with finite both MIPR and MNPR correspond to the mixed phases, and in between the system is in the localized phase with only finite MIPR. Delocalization indeed happens in the second mixed phase, and mobility edges emerge and disappear again as J_y increases [see the fourth panel in Fig. 2(b)].

After introducing two types of phase transitions, now we give phase diagrams that are decided by duality. To distinguish the mixed phase from extended and localized phases, we introduce the quantity [54,55]

$$\kappa = \log_{10}(\text{MIPR} \times \text{MNPR}). \tag{5}$$

In the extended phase, MIPR $\propto 1/L$, MNPR is finite, and $\kappa \propto \log_{10}(1/L)$. Similarly, MIPR is finite, MNPR $\propto 1/L$, and $\kappa \propto \log_{10}(1/L)$ in the localized phase. In the mixed phase containing extended and localized states in the spectrum, both MIPR and MNPR are finite, thus so is κ. In Fig. 3, we present the quantity κ in the $(\alpha(\beta), J_y)$ plane. When κ is very small, the system is in the extended phase (Ext) or localized phase (Loc), which is represented by blue areas. When κ is finite, the system is in the mixed phase (Mix) represented by an orange-red area. The two pictures are related by duality. To be more specific, if the system with (J_y, α, β) in (a) is in the localized (extended) phase, the system with $(\frac{1}{J_y}, \beta, \alpha)$ in (b) is in the extended (localized) phase, which is determined by duality even though the self-dual point does not exist. Besides, both phase diagrams are left-right symmetric, which is consistent with the theoretical analyses about the range of α and β in Sec. II.

Furthermore, we present the quantity κ in (β, J_y) plane for systems with different α in Fig. 4. Blue regions correspond to extended and localized phases, and the extended (localized) phase is at small (large) J_y. When $\alpha = 0$ or $\beta = 0$, the model can be decoupled into two copies of the classic AAH model, by rotations in the spin subspace [52]. Thus, the system undergoes an extended-localized phase transition

at $J_y = 1$, and the mixed phase is absent. In other cases, the non-Abelian gauge potential induces mixed phases between localized and extended/localized phases. The area of mixed phases in (β, J_y) plane increases first and decreases later as α increases. For a fixed α, the region of the mixed phases basically increases as β increases. Besides, the reentrant localization mainly happens when $\alpha \simeq \pi/4$ and $\beta \simeq \pi/4$.

IV. EXACT MOBILITY EDGES IN THE SEMICLASSICAL LIMIT $\Omega \ll 1$

Unlike in the noncomparable case with finite Ω, the localization of states can be analytically studied in the semiclassical limit. Given a single-particle eigenstate $|\Phi\rangle = \sum_{m\sigma} \phi_{m\sigma} \psi^\dagger_{m\sigma} |0\rangle$ with energy E, the Schrödinger equation of amplitudes $\phi_{m\sigma}$ is written as

$$\begin{bmatrix} \cos\alpha & \sin\alpha \\ -\sin\alpha & \cos\alpha \end{bmatrix} \begin{bmatrix} \phi_{m+1\uparrow} \\ \phi_{m+1\downarrow} \end{bmatrix} + \begin{bmatrix} \cos\alpha & -\sin\alpha \\ \sin\alpha & \cos\alpha \end{bmatrix} \begin{bmatrix} \phi_{m-1\uparrow} \\ \phi_{m-1\downarrow} \end{bmatrix} + \begin{bmatrix} 2J_y \cos\beta \cos(2\pi\Omega m) & -2J_y \sin\beta \sin(2\pi\Omega m) \\ -2J_y \sin\beta \sin(2\pi\Omega m) & 2J_y \cos\beta \cos(2\pi\Omega m) \end{bmatrix} \times \begin{bmatrix} \phi_{m\uparrow} \\ \phi_{m\downarrow} \end{bmatrix} = E \begin{bmatrix} \phi_{m\uparrow} \\ \phi_{m\downarrow} \end{bmatrix} \tag{6}$$

Then, applying the unitary transformation in the spin subspace,

$$\begin{bmatrix} \phi_{m\uparrow} \\ \phi_{m\downarrow} \end{bmatrix} = \frac{1}{\sqrt{2}} \begin{bmatrix} 1 & 1 \\ i & -i \end{bmatrix} \begin{bmatrix} \varphi_{m\uparrow} \\ \varphi_{m\downarrow} \end{bmatrix},$$

which does not affect spatial localization properties of states, plugging in the semiclassical condition that the quasiperiodic potential is slowly varying, explicitly $\cos[2\pi\Omega(m+1)] \approx \cos(2\pi\Omega m) \approx \cos[2\pi\Omega(m-1)]$, and annihilating one spin component by substituting one equation into the other, we obtain the equation of $\varphi_{m\downarrow}$:

$$\begin{aligned} &\varphi_{m+2\downarrow} + [4J_y \cos\alpha \cos\beta \cos(2\pi\Omega m) - 2E\cos\alpha]\varphi_{m+1\downarrow} \\ &\quad + \big[4J_y^2 \cos(2\pi\Omega m + \beta)\cos(2\pi\Omega m - \beta) \\ &\quad - 4J_y E \cos\beta \cos(2\pi\Omega m) + 2\cos(2\alpha) + E^2\big]\varphi_{m\downarrow} \\ &\quad + \big[4J_y \cos\alpha \cos\beta \cos(2\pi\Omega m) - 2E\cos\alpha\big]\varphi_{m-1,\downarrow} \\ &\quad + \varphi_{m-2\downarrow} = 0. \end{aligned} \tag{7}$$

A similar equation for the spin-$\uparrow$ component can be obtained too, which has the same localization behaviors as the spin-$\downarrow$ component. Assuming $\varphi_{m\downarrow} \propto Z^m$, the above equation becomes

$$(Z^2 + a_1 Z + 1)(Z^2 + a_2 Z + 1) = 0, \tag{8}$$

where $a_{1,2} = 2J_y \cos\alpha \cos\beta \cos(2\pi\Omega m) - E\cos\alpha \pm \sqrt{D}$ and $D = 4J_y^2 \sin^2\beta \sin^2(2\pi\Omega m) + 4\sin^2\alpha - \sin^2\alpha[E - 2J_y \cos\beta \cos(2\pi\Omega m)]^2$. The state is extended, if and only if, as $\cos(2\pi\Omega m)$ varies from -1 to 1, all complex roots Z of Eq. (8) are of unitary magnitude [32]. Otherwise, the state is localized as long as the magnitude of any one of the roots is not unitary. The prerequisite for the existence of an extended state or all unitary roots of Eq. (8) is that both $a_{1,2}$ are real; otherwise, the state is localized. Treating D as a quadratic function of one variable $\cos(2\pi\Omega m)$, one can find that $a_{1,2}$ are always real functions of $\cos(2\pi\Omega m) \in [-1, 1]$ when $\alpha = 0$ or $\alpha \neq 0$ and $|E| < 2 - 2J_y \cos\beta$. The calculation is straightforward. Once $a_{1,2}$ are real, the condition for all unitary roots of Eq. (8) is that both $|a_{1,2}| < 2$. When $\alpha = 0$ we obtain $a_{1,2} = 2J_y \cos(2\pi\Omega m \pm \beta) - E$. Given that β turns into global phases of quasiperiodic potentials, when $\alpha = 0$ Eq. (8) describes two decoupled copies of the classic AAH model with additional global phase shifts which do not affect the localization. $|a_{1,2}| < 2$ result in $|E| < 2 - 2J_y$. In the other case with $\alpha \neq 0$ and $|E| < 2 - 2J_y \cos\beta$, a straightforward calculation shows that $|a_{1,2}| < 2$ result in $0 \leqslant 2J_y - 2\cos\alpha < |E|$ when $\beta \neq 0$. Concluding all the above analyses, we obtain that states are extended when

$$\begin{aligned} &|E| < 2 - 2J_y && \text{for } \alpha\beta = 0, \\ &0 \leqslant 2J_y - 2\cos\alpha < |E| < 2 - 2J_y \cos\beta && \text{for } \alpha\beta \neq 0; \end{aligned} \tag{9}$$

otherwise, states are localized. Apparently, the model also supports mobility edges in the semiclassical limit. Exact expressions of the mobility edges are

$$|E| = 2 - 2J_y \tag{10}$$

when $\alpha\beta = 0$, and

$$|E| = 2J_y - 2\cos\alpha \quad \text{and} \quad |E| = 2 - 2J_y \cos\beta \tag{11}$$

when $\alpha\beta \neq 0$ and $0 < 2J_y - 2\cos\alpha < 2 - 2J_y \cos\beta$. There can be at most four mobility edges.

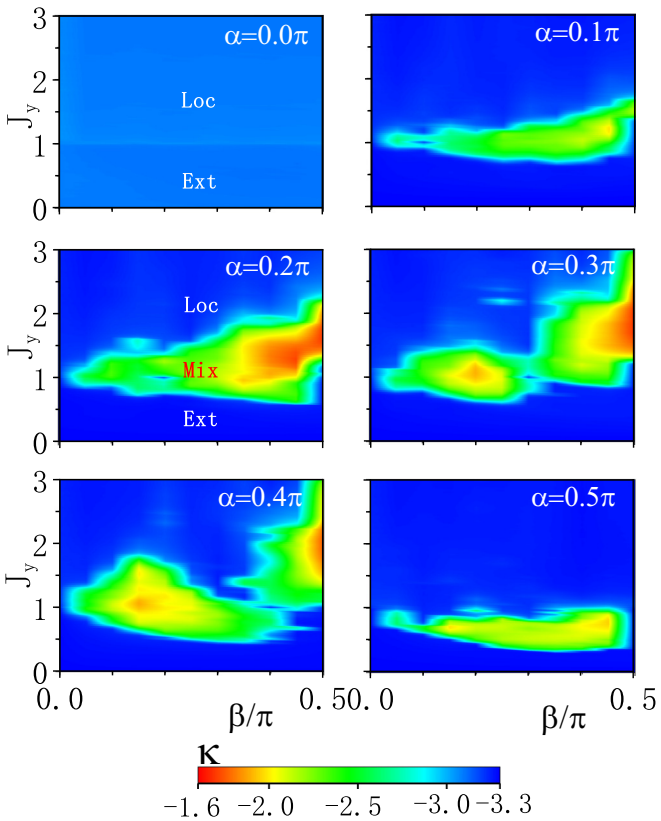

FIG. 4. Contour plot of the quantity κ in the (β, J_y) plane for systems with different α. $\Omega \simeq 610/987$ and $L = 987$.

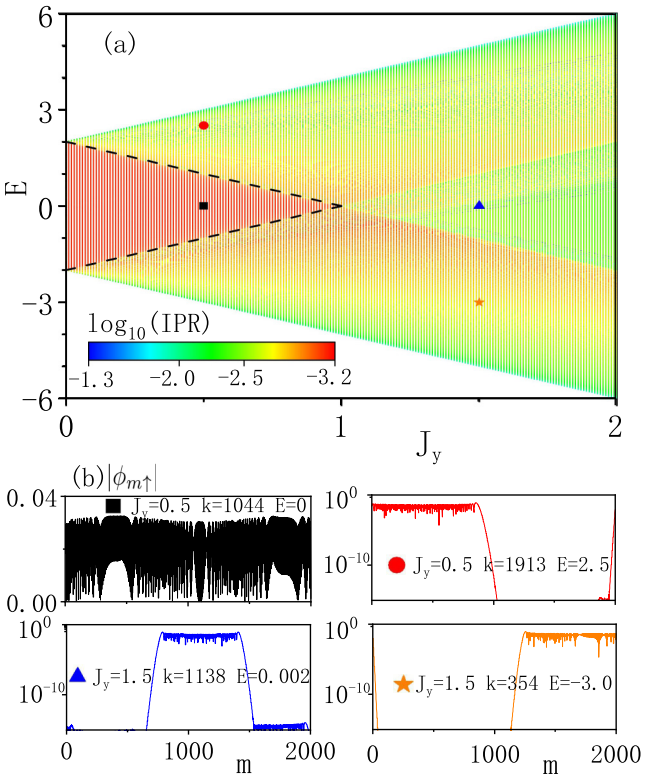

FIG. 5. (a) $\log_{10}$(IPRs) of single-particle states, as function of the corresponding energies E and quasiperiodic potential strength J_y, for systems with $\alpha = 0$ and $\beta = 0.3\pi$. The irrational $\Omega = \sqrt{2}/618\pi \ll 1$, and the total number of lattice sites $L = 1000$. (b) Typical spatial distributions of states, whose positions in spectra are shown in (a) (symbols).

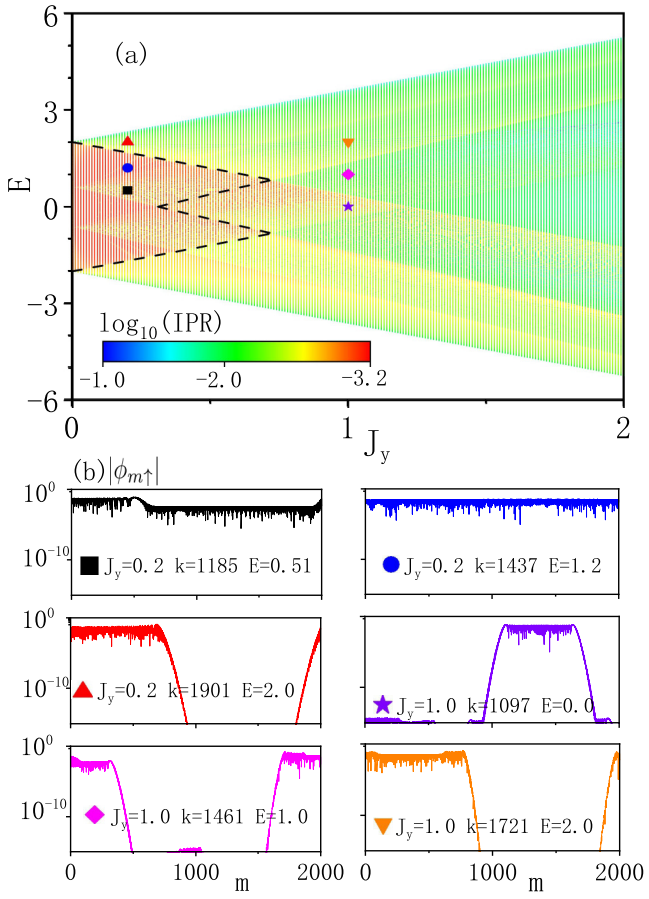

FIG. 6. (a) $\log_{10}$(IPRs) of single-particle states for systems with $\alpha = 0.4\pi$, $\beta = 0.2\pi$, $\Omega = \sqrt{2}/618\pi$, and $L = 1000$. (b) Semilogarithmic plots of spatial distributions of states, whose positions in spectra are shown in (a) (symbols).

The analytical results are consistent with numerical simulations. We first focus on the case $\alpha\beta = 0$, and in Fig. 5(a) we show a typical distribution of IPRs in the (J_y, E) plane. Unlike in the noncomparable case where due to the quasiperiodicity the spectrum splits into several subbands as J_y increases [see Fig. 1(a)], no splitting occurs in the semiclassical case. When J_y is small the system is in the mixed phase, consisting of a finite portion of extended and localized states. Extended states are at the center of spectra, i.e., in the middle of localized states. Critical states, separating extended and localized states and indicating localization phase transition, only exist on the lines of mobility edges, which are precisely described by Eq. (10) [black dashed lines in Fig. 5(a)]. To show localization of states, in Fig. 5(b) we show typical spatial distributions of states whose positions in spectra are indicated by symbols in Fig. 5(a). Differently from the ones in the noncomparable case, which decay exponentially from a localization center, here in the semiclassical case localized states have a finite extended region, and then away from the edge of the region they begin exponential decay. When $J_y > 1$, there seem to be also mobility edges, given that the IPRs experience sudden changes on extensions of the lines of exact mobility edges. As a matter of fact states are all localized when $J_y > 1$ [see spatial distributions of states indexed by triangle and star in Fig. 5(b)]. Maybe the sudden changes are from details of the localization of which we are unaware. Thus, when $J_y > 1$ the system is in the localized phase, and only when $J_y < 1$ do mobility edges exist and the system is in the mixed phase. The extended phase is absent as long as the quasiperiodic potential is present.

When $\alpha\beta \neq 0$ there are more than two mobility edges. In Fig. 6(a) we show an exemplary distribution of IPRs in the (J_y, E) plane, whose structure is more complicated than the one for $\alpha\beta = 0$. And in Fig. 6(b) we present spatial distributions of states in different regions whose positions in spectra are indicated by symbols in Fig. 6(a). Despite having different details—for example, in the distribution of the state indexed by square there is a region where the amplitude of state is basically smaller than that elsewhere, while the state indexed by the circle is basically uniformly distributed—all states on the left side of the black dashed lines, which correspond to the exact mobility edges, are extended, whereas all states on the right side of it are localized. The localization transition from the mixed to localized phases happens at $J_y = \frac{1+\cos\alpha}{1+\cos\beta}$, obtained from Eq. (11).

V. CONCLUSION AND DISCUSSION

We have studied localization properties of a generalized AAH model with a non-Abelian SU(2) gauge potential. The

localization crucially depends on the comparability between the quasiperiod and the lattice size. In the noncomparable case, when the strength of the quasiperiodic potential increases, the system undergoes a transition from the extended to mixed and then to localized phases. The system also hosts mobility edges in the mixed phase. Two mobility edges form at the center of the spectrum and move to the edges as the strength of the quasiperiodic potential increases. By carefully tuning strengths of the non-Abelian gauge potential, the system strikingly presents the reentrant localization transition, i.e., the extended-mixed-localized-mixed-localized phase transition. Mobility edges reemerge in the reentrant mixed phase. Furthermore, we have observed that the generalized AAH model retains the property of duality, and we have given the phase diagrams showing the duality.

On the other hand, in the semiclassical limit, the localization properties can be analytically obtained. When the strength of quasiperiodic potential increases, the system undergoes a transition from the mixed to localized phases at a critical strength which depends on strengths of the non-Abelian gauge potential. The extended phase is absent as long as the quasiperiodic potential is present. In the mixed phase, the exact expressions of the mobility edges have been analytically determined. There are two mobility edges when any one of the strengths of the non-Abelian gauge potential is zero; otherwise, there are four. Extended states locate at the middle of localized states, which is quite the opposite of the noncomparable case.

There we would like to mention that the localization physics discussed above can be experimentally tested. Before the dimensional reduction, the Hofstadter model can be realized in ultracold atoms, where the non-Abelian SU(2) gauge potential can be achieved by laser-assisted spin-dependent hopping [42,50,51]. The generalized AAH model can be realized in photonic waveguides. Photonic waveguides have been routinely used to demonstrate the localization of light [56,57]. In the tight-binding limit, propagation of classical light is governed by $i\,d\phi_j/dz = \kappa_j\phi_j + \sum_{l\neq j} t_{j,l}\phi_l$, which resembles the Schrödinger equation. κ_j is the refractive index of the jth waveguide, which plays the role of potential. $t_{j,l}$ is the hopping between different waveguides. In the ladder geometry, two legs correspond to two pseudospins and rungs play the role of lattice sites.

ACKNOWLEDGMENTS

We are supported by the NSFC Key Grant No. 12134015, and the NSFC Grants No. 11874393, No. 12175290, and No. 12121004.

[1] S. Aubry and G. André, Ann. Israel. Phys. Soc. **3**, 133 (1980).
[2] P. G. Harper, Proc. Phys. Soc. A **68**, 874 (1955).
[3] D. R. Hofstadter, Phys. Rev. B **14**, 2239 (1976).
[4] Y. E. Kraus, Y. Lahini, Z. Ringel, M. Verbin, and O. Zilberberg, Phys. Rev. Lett. **109**, 106402 (2012).
[5] L. J. Lang, X. Cai, and S. Chen, Phys. Rev. Lett. **108**, 220401 (2012).
[6] S. Ganeshan, K. Sun, and S. Das Sarma, Phys. Rev. Lett. **110**, 180403 (2013).
[7] S. Y. Jitomirskaya, Ann. Math. **150**, 1159 (1999).
[8] J. Sun, C. Wang, and J. Wang, Phys. Rev. B **46**, 12132 (1992).
[9] F. Evers and A. D. Mirlin, Rev. Mod. Phys. **80**, 1355 (2008).
[10] A. Lagendijk, B. Tiggelen, and D. S. Wiersma, Phys. Today **62**(8), 24 (2009).
[11] R. S. Whitney, Phys. Rev. Lett. **112**, 130601 (2014).
[12] C. Chiaracane, M. T. Mitchison, A. Purkayastha, G. Haack, and J. Goold, Phys. Rev. Res. **2**, 013093 (2020).
[13] V. Balachandran, S. R. Clark, J. Goold, and D. Poletti, Phys. Rev. Lett. **123**, 020603 (2019).
[14] M. Saha and S. K. Maiti, J. Phys. D: Appl. Phys. **52**, 465304 (2019).
[15] M. Saha and S. K. Maiti, Physica E **93**, 275 (2017).
[16] H. Yin, J. Hu, A.-C. Ji, G. Juzeliūnas, X.-J. Liu, and Q. Sun, Phys. Rev. Lett. **124**, 113601 (2020).
[17] T. Kohlert, S. Scherg, X. Li, H. P. Lüschen, S. Das Sarma, I. Bloch, and M. Aidelsburger, Phys. Rev. Lett. **122**, 170403 (2019).
[18] K. Yamamoto, A. Aharony, O. Entin-Wohlman, and N. Hatano, Phys. Rev. B **96**, 155201 (2017).
[19] S. Roy, T. Mishra, B. Tanatar, and S. Basu, Phys. Rev. Lett. **126**, 106803 (2021).
[20] X. Deng, S. Ray, S. Sinha, G. V. Shlyapnikov, and L. Santos, Phys. Rev. Lett. **123**, 025301 (2019).
[21] L. Zhou, H. Pu, and W. Zhang, Phys. Rev. A **87**, 023625 (2013).
[22] M. Kohmoto and D. Tobe, Phys. Rev. B **77**, 134204 (2008).
[23] J. Biddle, B. Wang, D. J. Priour Jr., and S. Das Sarma, Phys. Rev. A **80**, 021603(R) (2009).
[24] H. Yao, A. Khoudli, L. Bresque, and L. Sanchez-Palencia, Phys. Rev. Lett. **123**, 070405 (2019).
[25] M. Saha, S. K. Maiti, and A. Purkayastha, Phys. Rev. B **100**, 174201 (2019).
[26] Y. Wang, X. Xia, L. Zhang, H. Yao, S. Chen, J. You, Q. Zhou, and X.-J. Liu, Phys. Rev. Lett. **125**, 196604 (2020).
[27] J. Biddle and S. Das Sarma, Phys. Rev. Lett. **104**, 070601 (2010).
[28] S. Ganeshan, J. H. Pixley, and S. Das Sarma, Phys. Rev. Lett. **114**, 146601 (2015).
[29] J. D. Bodyfelt, D. Leykam, C. Danieli, X. Yu, and S. Flach, Phys. Rev. Lett. **113**, 236403 (2014).
[30] T. Liu, S. Cheng, R. Zhang, R. Ruan, and H. Jiang, Chin. Phys. B **31**, 027101 (2022).
[31] S. Das Sarma, S. He, and X. C. Xie, Phys. Rev. Lett. **61**, 2144 (1988).
[32] T. Liu and H. Guo, Phys. Rev. B **98**, 104201 (2018).
[33] Q. Tang and Y. He, J. Phys.: Condens. Matter **33**, 185505 (2021).
[34] Z. Lu, Z. Xu, and Y. Zhang, Ann. Phys. (Berlin) **534**, 2200203 (2022).
[35] Y. Wang, J.-H. Zhang, Y. Li, J. Wu, W. Liu, F. Mei, Y. Hu, L. Xiao, J. Ma, C. Chin, and S. Jia, Phys. Rev. Lett. **129**, 103401 (2022).
[36] G. Roati, C. D'Errico, L. Fallani, M. Fattori, C. Fort, M. Zaccanti, G. Modugno, M. Modugno, and M. Inguscio, Nature (London) **453**, 895 (2008).

[37] H. P. Lüschen, S. Scherg, T. Kohlert, M. Schreiber, P. Bordia, X. Li, S. Das Sarma, and I. Bloch, Phys. Rev. Lett. **120**, 160404 (2018).
[38] V. Goblot, A. Štrkalj, N. Pernet, J. L. Lado, C. Dorow, A. Lemaître, L. L. Gratiet, A. Harouri, I. Sagnes, S. Ravets, A. Amo, J. Bloch, and O. Zilberberg, Nat. Phys. **16**, 832 (2020).
[39] F. A. An, K. Padavić, E. J. Meier, S. Hegde, S. Ganeshan, J. H. Pixley, S. Vishveshwara, and B. Gadway, Phys. Rev. Lett. **126**, 040603 (2021).
[40] F. A. An, E. J. Meier, and B. Gadway, Phys. Rev. X **8**, 031045 (2018).
[41] Y. Lahini, R. Pugatch, F. Pozzi, M. Sorel, R. Morandotti, N. Davidson, and Y. Silberberg, Phys. Rev. Lett. **103**, 013901 (2009).
[42] N. Goldman, A. Kubasiak, A. Bermudez, P. Gaspard, M. Lewenstein, and M. A. Martin-Delgado, Phys. Rev. Lett. **103**, 035301 (2009).
[43] E. Zohar, J. I. Cirac, and B. Reznik, Phys. Rev. Lett. **110**, 125304 (2013).
[44] E. Zohar, J. I. Cirac, and B. Reznik, Rep. Prog. Phys. **79**, 014401 (2016).
[45] V. Galitski, G. Juzeliūnas, and I. B. Spielman, Phys. Today **72**(1), 38 (2019).
[46] I. Raychowdhury, Indian J. Phys. **95**, 1681 (2021).
[47] R. Dasgupta and I. Raychowdhury, Phys. Rev. A **105**, 023322 (2022).
[48] L. Tagliacozzo, A. Celi, P. Orland, M. W. Mitchell, and M. Lewenstein, Nat. Commun. **4**, 2615 (2013).
[49] E. G. Guan, H. Yu, and G. Wang, Phys. Lett. A **384**, 126152 (2020).
[50] J. M. Hou, W. X. Yang, and X. J. Liu, Phys. Rev. A **79**, 043621 (2009).
[51] A. Bermudez, L. Mazza, M. Rizzi, N. Goldman, M. Lewenstein, and M. A. Martin-Delgado, Phys. Rev. Lett. **105**, 190404 (2010).
[52] M. Rossignolo and L. Dell'Anna, Phys. Rev. B **99**, 054211 (2019).
[53] Y. Wang, Y. Wang, and S. Chen, Eur. Phys. J. B **89**, 254 (2016).
[54] X. Li and S. Das Sarma, Phys. Rev. B **101**, 064203 (2020).
[55] C. Wu, J. Fan, G. Chen, and S. Jia, New J. Phys. **23**, 123048 (2021).
[56] T. Schwartz, G. Bartal, S. Fishman, and M. Segev, Nature (London) **446**, 52 (2007).
[57] Y. Lahini, A. Avidan, F. Pozzi, M. Sorel, R. Morandotti, D. N. Christodoulides, and Y. Silberberg, Phys. Rev. Lett. **100**, 013906 (2008).